

Neural Networks and Friction: Slide, Hold, Learn

Joaquin Garcia-Suarez^{a)}

*Institute of Civil Engineering, École Polytechnique Fédérale de Lausanne (EPFL)
CH 1015 Lausanne, Switzerland*

(Dated: 17 June 2024)

In this study, it is demonstrated that Recurrent Neural Networks (RNNs), specifically those utilizing Gated Recurrent Unit (GRU) architecture, possess the capability to learn the complex dynamics of rate-and-state friction laws from synthetic data. The data employed for training the network is generated through the application of traditional rate-and-state friction equations coupled with either the aging law or the for state evolution. A novel aspect of our approach is the formulation of a loss function that explicitly accounts for the direct effect by means of automatic differentiation. It is found that the RNN, with its GRU architecture, effectively learns to predict changes in the friction coefficient resulting from velocity jumps (with and without noise in the target data), thereby showcasing the potential of machine learning models in capturing and simulating the physics of frictional processes.

Keywords: friction, rate-and-state-dependent friction, neural networks, recurrent neural networks, GRU

I. INTRODUCTION

Understanding the dynamics of friction is paramount across several disciplines, including mechanical engineering, civil engineering, and geophysics^{1,2}. In mechanical and civil engineering, precise knowledge of frictional forces is crucial for the design and analysis of machines, structures, and materials under varying operational conditions³⁻⁶. In geophysics, friction dynamics play a critical role in earthquake mechanics, influencing the initiation, propagation, and arrest of seismic slips along faults⁷.

Numerous models have been proposed to describe frictional behavior, from classical laws like Amontons-Coulomb friction², which simplifies friction as a constant proportion of the normal load, to much more complex ones. However, these models often fall short in capturing the full range of observed behaviors^{7,8}.

Rate-and-state friction (RSF) laws stand out by explicitly addressing the velocity and time-dependent effects, thereby providing a more comprehensive framework for understanding the seismic cycle⁹. A customary expression of this law is⁷:

$$\mu = \mu_0 + a \ln \left(\frac{V}{V_{ref}} \right) + b \ln \left(\frac{V_{ref} \theta}{D_c} \right), \quad (1)$$

where μ is the friction coefficient, μ_0 is the friction coefficient at a reference velocity V_{ref} , V is the sliding velocity, and a is a positive constant representing the direct effect's sensitivity to velocity changes¹⁰, b is a constant that, along with a , determines the frictional response to changes in sliding velocity and state evolution¹¹.

Friction modeling^{12,13} aims to capture essential features observed in experimental settings¹⁴, notably the direct effect and healing².

Healing, also referred to as state evolution effect, illustrates the time-dependent increase in frictional resistance during stationary contact, attributed to the contact area's growth at asperity contacts or chemical bonding at the interface². This process is often modeled by the evolution of an internal variable θ (termed "state"), with the simplest form being the "aging law" and the "slip law":

$$\dot{\theta} = \frac{d\theta}{dt} = 1 - \frac{\theta V}{D_c}, \quad (2a)$$

$$\dot{\theta} = \frac{d\theta}{dt} = -\frac{\theta V}{D_c} \log \left(\frac{\theta V}{D_c} \right), \quad (2b)$$

where t is time and D_c is a critical slip distance over which the state variable evolves significantly¹⁵. In the aging law, the state is interpreted as a measure of effective age of contacts between the asperities of the opposed surfaces^{10,16}, a logical position given that contact area between two rough surfaces is also to grow logarithmically over time during periods of rest or very slow sliding^{5,17}. Notwithstanding this intuitive inference, the slip law offers a picture that may be better backed by experiments^{18,19}, in which the sensitivity to sliding does not ever disappear, not even at tiny sliding rates¹⁹.

Despite their advantages, RSF laws are not without limitations. Identifying the parameters a , b , and D_c from experimental data poses significant challenges due to the complex interplay between different physical processes at the frictional interface⁷.

Criticism has been levied against the use of the "state" variable in RSF laws for its lack of a clear physical basis, leading to calls for models that include more explicit physical mechanisms^{20,21}. For example, the parameters that appear in eq. (1) are assumed to be constants, and they may not²²⁻²⁶. Furthermore, the need to regularize these laws to address numerical instabilities



FIG. 1 Artistic representation of the magnified rough interface between two plates in sliding contact, where asperities grinding give rise to debris particle formation.

and ensure the physical consistency of simulations has been highlighted^{27,28}. Recently, laboratory²⁹ and virtual experiments^{30,31} have shown the limitations of RSF laws even in highly controlled interface conditions.

Given these challenges and the limitations of existing models, there is a clear need to explore new methodologies for understanding friction dynamics. This necessity is particularly acute for modeling phenomena that span multiple scales of time and space³². Herein lies the potential of novel data-driven approaches, such as Recurrent Neural Networks (RNNs)³³, to offer new insights and overcome the limitations of traditional friction laws.

Neural networks have revolutionized the field of machine learning, offering powerful tools for modeling complex, non-linear relationships in data across a myriad of disciplines³⁴. At their core, neural networks are composed of layers of interconnected nodes or “neurons”, each capable of performing simple computations. Through the process of training, these networks adjust their internal parameters to minimize the difference between their output and the desired outcome, effectively learning to map inputs to outputs³⁵.

Among the various architectures of neural networks, Recurrent Neural Networks (RNNs) stand out for their ability to process sequential data. Unlike feedforward neural networks, RNNs possess a form of memory that allows them to incorporate information from previous inputs into the current processing step³⁶. This characteristic makes RNNs particularly suited for tasks involving time series data or any context where the sequence of data points is crucial.

Two notable advancements in RNN architecture are the Gated Recurrent Unit (GRU) and Long Short-Term Memory (LSTM) networks. Both GRU and LSTM address a fundamental limitation of basic RNNs known as the vanishing gradient problem associated to recurrent connections³³, which makes it difficult for RNNs to learn dependencies between events that occur at long intervals in the input data^{35,37}. GRUs simplify the LSTM architecture while retaining its ability to capture long-term

dependencies, making it both efficient and powerful for a wide range of tasks³⁶.

The application of RNNs, GRUs, and LSTMs has been widespread and transformative across many fields, including physics³⁸. Particularly, their success in modeling path-dependent plasticity of materials highlights their potential^{39–46}. Path-dependent plasticity is a critical aspect in the study of materials science, where the history of material deformation affects its current and future state. RNNs have been shown to effectively model these complex relationships, capturing the history-dependent nature of material behavior^{47,48}.

This success in modeling path-dependent phenomena provides a strong foundation for the belief that similar methodologies can be applied to the study of friction. Friction, much like material plasticity, is inherently dependent on history, in its case of contact and slip between surfaces. The capability of RNNs to capture and learn from sequential, history-dependent data makes them promising candidates for advancing modeling of friction dynamics.

The goal of this short communication is to show that RNNs, based on GRUs, can perform at least *as well as* RSF laws based on either the aging law, eq. (2a), or the slip law eq. (2b). This approach is essentially different from the one used recently by Ishiyama and collaborators⁴⁹, who used machine learning (random forest⁵⁰) to improve the estimation of RSF parameters eq. (1); herein, machine learning is not deployed to improve an empirical approximate law, but to replace it altogether; down the road, we envision neural-network frictional models being embedded in larger-scale simulations^{21,51,52}. It also differs from the use made by Rouet-Leduc *et al*⁵³ and Hulbert *et al*⁵⁴, among others^{55,56}, who used machine learning techniques to devise impending rupture predictions based on acoustic emissions recorded in lab settings. To the best of my knowledge, the closest work to ours may be the one by Wang and Sun⁵⁷, which focused on interfacial traction-opening laws, and the recent one by Cravero and K. Bhattacharya⁵⁸, who studied interface adhesion. Herein, we assume a virtual interface that is perfectly modeled by a customary aging and slip laws, eqs. (1), (2a) and (2b), for which data for training and verification can be generated easily from those equations. We use those data to train a GRU network with a custom loss function to learn the dynamics without explicitly defining internal variables⁴⁷, since the state is not a physical quantity that can be measured experimentally, cf. work by Kumar and collaborators^{59,60}. In reality, the complexities of interface physics⁶¹ are such that probably no single internal variable can be defined as long as one aims at capturing any ambitious degree of complexity. We presume implicitly that sliding amount and sliding rate are the sole driving forces of the phenomenon, and whatever internal variables there may be can be internally codified in the hidden states of the net. The figure of merit will not be the dynamic friction coefficient itself, but *variations in*

the friction coefficient due to sliding. This decision is motivated by the practical inability to surmise the time evolution of the friction coefficient except if proper initial conditions are supplied. Hence, when using the trained network to make predictions, one should picture an on-going experiment that has reached a certain steady-state friction level: that information and the subsequent velocity protocol are passed to the network, which outputs a prediction for the friction evolution for the rest of the experiment.

The structure of the paper is as follows: the methods section (II) introduces the GRU architecture (emphasizing how it encodes internal variable evolution), describes the generation of synthetic data for training and verification, and explains the choice of training hyperparameters, including the physics-informed loss function. The next section (III) describes the outcome of the training process, which details performance evaluation, and IV then assesses the model’s predictive accuracy on independent datasets. The discussion section (V) analyzes the findings and their implications. The final remarks section (VI) summarizes the study’s contributions and suggests future research directions.

II. METHODS

II.A. Neural networks for sequences: gated recurrent units

RNNs are engineered to handle sequential data thanks to their ability to maintain a memory of previous inputs by feeding the output of a neuron back onto itself³³. This recursive nature allows making predictions based on the information accumulated from prior inputs. However, standard RNNs often struggle with long-term dependencies due to the vanishing gradient problem³⁵, where back-propagation gradients become too small or too large (over successive passings through a loop) for the network to learn effectively over many time steps³³.

Gated Recurrent Units (GRUs) are an evolution of the traditional RNN architecture, designed to mitigate the vanishing gradient problem and improve the network’s ability to learn from long sequences. GRUs introduce gated units that control the flow of information. These gates “decide” which information is relevant to keep or discard as the sequence progresses, enabling the network to maintain a longer memory, which will be useful here to handle evolution of internal variables.

The GRU mechanism is articulated mathematically through³⁶ the following variables:

$$r_t = \sigma(W_{ir}x_t + b_{ir} + W_{hr}h_{t-1} + b_{hr}) \quad (3a)$$

$$z_t = \sigma(W_{iz}x_t + b_{iz} + W_{hz}h_{t-1} + b_{hz}) \quad (3b)$$

$$n_t = \tanh(W_{in}x_t + b_{in} + r_t \odot (W_{hn}h_{t-1} + b_{hn})) \quad (3c)$$

$$h_t = (1 - z_t) \odot n_t + z_t \odot h_{t-1}, \quad (3d)$$

where:

- h_t is the hidden state at time t , playing a role analogous to $\theta(t)$,

- x_t is the input at time t (in our case corresponds to $V(t)$),
- h_{t-1} is the hidden state of the layer at time $t - 1$ (the loop should play the role of solving eq. (1)),
- r_t, z_t, n_t are the reset, update, and new gates, respectively,
- σ is the sigmoid function, and
- \odot is the Hadamard product.

II.B. Synthetic data generation

It is assumed that the state θ will not be needed by the neural network that is to replace the traditional RSF law; the internal interface evolution will be handled by h_t . This means that there will not be vectors of values of θ being used during training, but it does not imply that eqs. (2a) and (2b) are not being used during the datasets’ generation. Let us reiterate that we assume the hypothetical interface that is perfectly described by eq. (1), but this fact would be hidden to us if we were to analyze experimental data coming out of that interface. Having access directly to the friction coefficient is common to gouge experiments, yet not so much in other settings (e.g., PMMA friction experiments) which display more complex dynamics as stick-slip. The latter will be addressed in future work.

So, to generate the dataset for training and verifying our model, we start by defining a traditional RSF model with specific parameter values, grounded in the fundamental equations presented earlier, with particular parameter values set as follows:

- Friction coefficient, $\mu_0 = 0.5$ (unitless)
- Rate-state parameter, $b = 0.015$ (unitless)
- Direct effect parameter, $a = 0.005$ (unitless)
- Reference velocity, $V_{\text{ref}} = 1.0 \cdot 10^{-4}$ m/s
- Characteristic slip distance, $D_c = 2.0 \cdot 10^{-4}$ m

Using these values, we simulate 13000 random sequences to reflect diverse frictional sliding scenarios. The prior experiences with material plasticity learning^{39,42,44} suggested that using random forcing to generate the datasets is advisable. Each sequence is designed to simulate a total sliding distance of $30D_c$ and is completed within 0.013 seconds. The number of velocity jumps within each sequence is randomly determined, drawing from a uniform distribution with values 2, 3, 4, 5. It is assumed that each sequence initiates from a non-zero velocity, with the initial state of the interface corresponding to the steady state for that velocity, as defined by the RSF laws: $\theta_{ss} = D_c/V(t=0)$.

Velocity jumps within these sequences occur at random intervals, determined by sampling times from a uniform distribution across the interval 0, 1, with 0 marking the start and 1 the end of the sliding protocol. Each sequence incorporates a hold period where the velocity drops to

zero, simulating intervals where sliding stops until the subsequent jump. To avoid issues associated to dividing by zero or trying to compute the logarithm of either zero or negative numbers, a small yet finite velocity is assigned to the hold for computations ($2 \cdot 10^{-9}$ m/s for aging law, $2 \cdot 10^{-3}$ m/s for slip law).

To compute the velocities between jumps, we divide the total sliding distance by the time spans between these jumps, ensuring that the velocities remain constant in these intervals. Thus, we define the “velocity protocol” for each sequence / virtual experiment.

Having the velocity protocol, we proceed to calculate the evolution of the state variable θ using either eq. (2a) or eq. (2b), and initial conditions $V(t = 0) = V_0$ and $\theta(t = 0) = \theta_{ss}$. With the velocity protocol and the evolving state variable at hand, we can then compute the friction coefficient’s evolution over time, as described by the RSF models (eq. (1)).

The dataset comprises pairs of “features” and “targets”. Features represent the velocity protocol sampled at 100 equally-spaced instants during the duration of each virtual experiment, while targets correspond to *variations with respect to the initial value* of the friction coefficient sequence at these same instants. The reason for working with variations and not with the actual values of friction coefficient is that there is no way to predict the *initial* values of friction based on these datasets, they have to be provided as initial conditions over which the variations are later superimposed. There is the implicit assumption (borne by empirical observations) that the variations depend on sliding velocity, but not on the instantaneous magnitude of the friction coefficient.

For training, we normalize using the following characteristic values: $\delta\mu_{ch} = 0.01$ for the friction coefficient change and $V_{ch} = 0.3$ m/s for the velocities. 10% of the sequences are put aside to test the network once it is trained.

When it comes to adding noise to the targets $\delta\mu_{ch}$, we choose Gaussian noise with standard deviation 0.005 and zero mean.

II.C. Network details

The pyTorch python neural networks package⁶² has been used.

II.C.1. Architecture

The main net, which is aimed at replacing eq. (1) and whose parameters must be learned via training, is made up by a single GRUNet, followed by a folded Linear layer to transforms the output of the GRU through a linear transformation.

II.C.2. Training parameters

We employ the ADAM optimization method⁶³. A learning rate of 0.001 is chosen as it is generally con-

sidered a good default and has been proven effective across a wide range of tasks. We choose to initially use a batch size of 32 when using most of the data for training, then batch sizes of 10 or just 1 sequence were used, respectively, when training with only 1000 or 100 sequences. Finally, during training we use a maximum of 1000 epochs combined with early stopping (the training is terminated if the loss does not improve after 20 epochs, for larger datasets, or 50 epochs, for smaller ones), combined with gradient clipping to avoid erratic exploration of the loss landscape (maximum magnitude 1), and saving the weights yielding the minimum loss to be the ones used later in inference mode.

II.C.3. Loss function

The aphorism “the Law is a teacher” is often attributed to Saint Augustine of Hippo^{64,65}, an early Christian philosopher. In the case of neural networks, “the loss is the teacher”. Inspired by physics-informed neural networks (PINNs)³⁸, we devise a loss function that takes advantage of automatic differentiation⁶⁶ and reflects physical principles to guide the optimization of the parameters of the network.

Let $\delta\mu$ and $\delta\hat{\mu}$ represent the vector of normalized predictions and targets (respectively) for a given vector of features (velocity protocol) \mathbf{V} , i.e., $\delta\mu = \text{NN}(\mathbf{V}/V_{ch})$. See that $\delta\mu, \delta\hat{\mu}, \mathbf{V} \in \mathbb{R}^N$ (and $N = 100$ in this case). The first part of the loss is the mean-absolute error (MAE):

$$\text{loss}_1 = \frac{\|\delta\mu - \delta\hat{\mu}\|}{N}, \quad (4)$$

where $\|\cdot\|$ represents the L_1 norm of the vector. This term leads the parameter adjustment during training to follow the available data as closely as possible. The extra loss terms are aimed to choose among the many ways that there are to minimize this average error.

The second part of the loss represents the difference between the initial values of predictions and targets,

$$\text{loss}_2 = |\delta\mu_1 - \delta\hat{\mu}_1|, \quad (5)$$

where the sub-index 1 refers to the first element of every sequence. This term will be useful to stabilize the first predictions, but will be deactivated if there is noise in the target data.

To further stabilize the initial prediction, we also enforce the initial gradient to be zero:

$$\text{loss}_3 = \frac{\partial(\delta\mu_1)}{\partial V}, \quad (6)$$

since the velocity should not change in the first step. The conditions that experimental evidence impose over the friction coefficient are the direct effect, i.e., logarithmic dependence of velocity magnitude, and healing, i.e., logarithmic increase of the static friction coefficient with time (during holds)

$$\frac{\partial\mu}{\partial \log V} = c_1, \quad \frac{\partial\mu_s}{\partial \log t} = c_2, \quad (7)$$

where μ_s is the static friction coefficient, c_1 and c_2 are interface-dependent constants. According to eq. (1), the direct effect is controlled by a and healing by $(a - b)$, but we are assuming we do not know that the interface is modeled by these parameters, so shall impose that the change of these relative variations is constant, not that the variations themselves are of a given magnitude.

The third term of the loss is meant to enforce the direct effect: a sudden peak in friction induced by a jump in leading velocity (which, moreover, is known to be proportional to the logarithm of the ratio of velocities before and after the jump, see section I). First, we note that the logarithmic dependence implicit in eq. (7) is equivalent to

$$\Delta \left[V \frac{\partial \mu}{\partial V} \right]_{t_1, t_2} = \left(\left[V \frac{\partial \mu}{\partial V} \right]_{t_1} - \left[V \frac{\partial \mu}{\partial V} \right]_{t_2} \right) = 0, \quad (8)$$

for any two successive instants t_1 and t_2 , the derivatives at either time can be efficiently computed using the automatic differentiation capabilities of pyTorch. Assuming that the training data has enough resolution to capture every velocity jump, we can safely choose t_1 and t_2 to be any two consecutive points, and we must have that the logarithmic increment to be zero to ensure that the variations of the friction coefficient with respect to velocity happens in logarithmic fashion. Since that should be the case for every two successive data points, the loss term for direct effect must be

$$\text{loss}_4 = \sum_{i=1}^{N-1} \Delta \left[V \frac{\partial(\delta\mu)}{\partial V} \right]_{t_i, t_{i+1}}. \quad (9)$$

The terms corresponding to holds should not enter the previous sum, as there the dominant phenomenon is not the direct effect but healing. Conveniently, the fact that $V \approx 0$ during holds automatically acts as a “mask”³³, effectively removing those terms from the loss.

Finally, let us address healing. Since none of the two laws feature exactly logarithmic evolution and they assign different values of static friction, it was decided (after some tests, see appendix A) that it works better to leave the network to learn this behavior directly from the minimization of the average error. Future work will be occupied with tailoring the architecture, the training or both to deal with this phenomenon.

The overall loss term that guides the optimization of weights and biases during the training process is:

$$\text{loss} = \lambda_1 \text{loss}_1 + \lambda_2 \text{loss}_2 + \lambda_3 \text{loss}_3 + \lambda_4 \text{loss}_4, \quad (10)$$

$\alpha, \beta, \gamma \in \mathbb{R}$. It has been found that $\lambda_1 = 1$, $\lambda_2 = \lambda_3 = 0.1$ ($\lambda_2 = 0$ whenever noise is present) and $\lambda_4 = 0.01$ yield satisfactory results. When dealing with noisy data, an extra L2-regularization term is added, with $\lambda_{\text{reg}} = 10^{-4}$.

III. TRAINING RESULTS

For illustration purposes, the overall training procedure is depicted in fig. 2 and the final losses are consigned

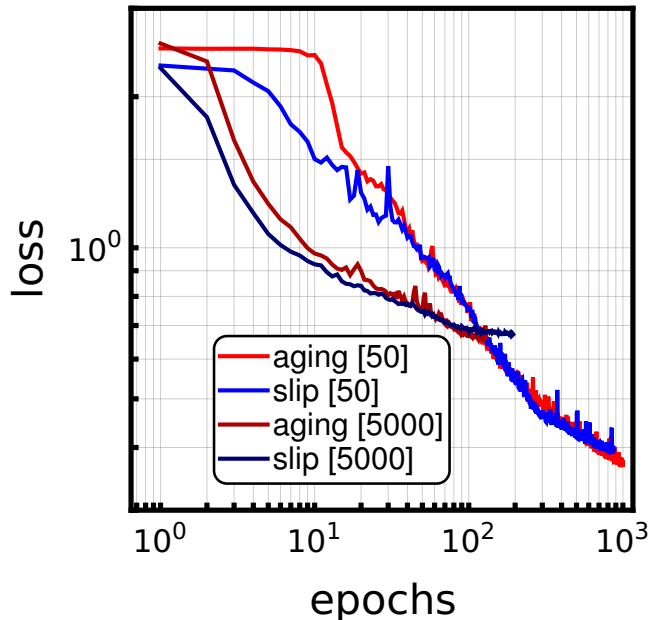


FIG. 2 Loss during training: aging and slip laws, for 50 training experiments and 5000.

in table I only for the noiseless data. The same loss function was used, but the batch size was changed: 32 for 10000 sequences, 10 for 1000 and 1 for both 100 and 10. This just means that the weights and biases were updated more often the smaller the dataset. For each dataset size, the loss can be reduced to the same final value by tuning this parameter. Similar trends are observed for the noisy data, both for the slip and aging laws. Remarkably, to attain that loss level with noisy data one was to train for many more epochs (~ 1000) and the early-stop parameter (“patience”) has to be increased to 50.

TABLE I Using the aging law and noiseless data: final loss value and validation error for different training dataset sizes.

| Training Dataset Size | 10^1 | 10^2 | 10^3 | 10^4 |
|-----------------------|--------|--------|--------|--------|
| Minimal Loss | 0.17 | 0.11 | 0.08 | 0.11 |
| Average Error (%) | 4.6 | 1.2 | 0.62 | 0.67 |

TABLE II Average validation error (%) for different training dataset sizes (test dataset corresponds to sequences generated with the aging law): comparison aging and slip laws (same architecture and training hyperparameters).

| Training Dataset Size | 10^1 | 10^2 | 10^3 | 10^4 |
|-----------------------|--------|--------|--------|--------|
| Aging | 7.2 | 1.9 | 2.2 | 1.0 |
| Slip | 4.42 | 2.9 | 3.7 | 2.5 |

IV. TEST

Once the training is complete, we take out the main net, which is our ready-to-use NN function that is to model the interface evolution. We test it using the 3000

sequences, generated with the aging law eq. (2a), that no net saw during training. For each sequence, the percent error is computed as

$$\text{error}(\%) = 100 \frac{\|\text{NN}(\mathbf{V}/V_{ch}) - \delta\hat{\boldsymbol{\mu}}/\delta\mu_{ch}\|_2}{\|\delta\hat{\boldsymbol{\mu}}/\delta\mu_{ch}\|_2}, \quad (11)$$

the underlying truth is considered to be the noiseless data (this also helps to verify the lack of overfitting).

The mean test error (averaged over the 3000 sequences) is consigned in table I for noiseless data (only aging law) and in table II for noisy data (both aging and slip laws). For noiseless data, the error is approximately 50% smaller

V. DISCUSSION

As hinted by the test results presented in tables I and II, figs. 3 to 5 clearly showcase that the GRU-based networks are able of closely reproducing the friction dynamics encapsulated in the datasets generated with a customary rate-and-state phenomenological law. Remarkably, the aforementioned tables and plots evince that reasonable amounts of training data (~ 100 experiments) are enough for the network to learn the dynamics. This is a promising result, since the next step in this research effort is to learn from laboratory experiments, which are much more limited in number.

Clearly, the loss term associated to logarithmic velocity dependence, eq. (9), is doing its part in concentrating gradients where the sudden changes in velocity magnitude are detected without compromising the transient evolution after velocity steps.

Nevertheless, there still are obvious limitations. First, fig. 3 reveals that the network trained with slip-law data struggles to capture the direct effect right after the hold, no matter how much training data is available. Conversely, the network whose parameters were adjusted with aging-law datasets performs much better, see fig. 4. Their different performance is also illustrated by fig. 5. Therein, for the same amounts of training data (just 100 sequences) the aging-trained model captures better the drop in friction when hold starts and the peak after re-sliding. This behavior could be explained by the fact that the slip-law training data assigns the same value to the static coefficient when the hold starts regardless of the prior dynamic magnitude¹⁹, while this value changes as a function of that magnitude in the case of the aging law. Hence, this may build extra flexibility in the aging-trained net.

The previous discussion highlights the need to develop more tailored loss functions to better account for healing.

VI. FINAL REMARKS

This study has demonstrated that recurrent neural networks based on Gated Recurrent Units (GRUs) possess the capability to accurately model slide-hold protocols in the context of rate-and-state friction laws, provided that the networks are supplied with adequate data and the loss

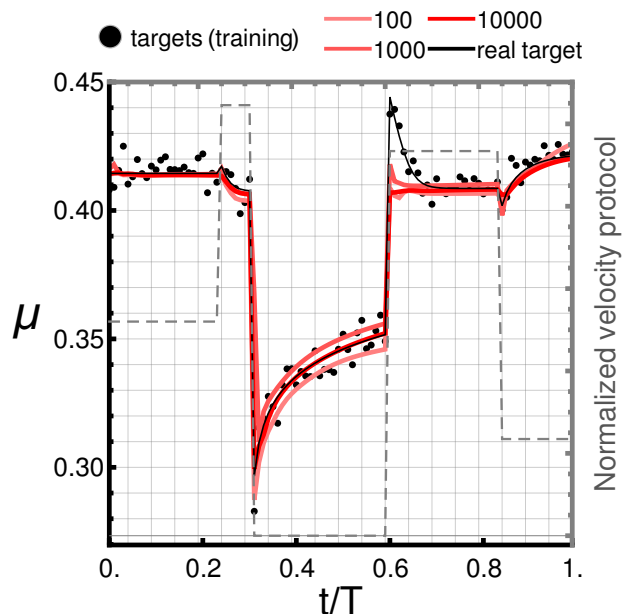


FIG. 3 Test example #1: light right axis for loading velocity, dark right axis for friction coefficient evolution. Emphasis on capacities of neural network based on slip-law datasets (100, 1000 and 10000 sequences). The dashed background line represents the velocity protocol.

function is tuned accordingly. These findings affirm the potential of recurrent neural networks as a promising tool for understanding complex frictional behavior, showcasing their ability to learn from and predict the dynamics of friction with high fidelity. This success highlights the ability of deep learning approaches to replace customary phenomenological laws for dynamic friction, additionally avoiding the need to explicitly define internal variables. Another reason to be optimistic is that there are still improvements to be explored when it comes to tailor both the architecture (going beyond “off-the-self” GRU cells) and the training procedure.

However, our investigation also identified limitations. Particularly, we observed a potential conflict between optimizing for healing and for the direct effect within the training process, indicating an area for further refinement in how these fundamental aspects of frictional behavior are integrated into the learning scheme. Moreover, even though I considered both noiseless and noisy data, the levels of synthetic noise may not be representative of the intrinsic variability that one may expect in laboratory settings.

This document contains but an exploratory approach to modeling frictional interface via deep learning. Looking forward, there are several avenues for enhancing the predictive power and generalizability of recurrent neural networks for dynamic friction. Improvement could be sought through the addition of more nuanced physics-informed loss functions predicated on thermodynamic principles^{43,46} and exploration of alternative or *ad hoc*^{39,47} RNN architectures). Further parametric studies

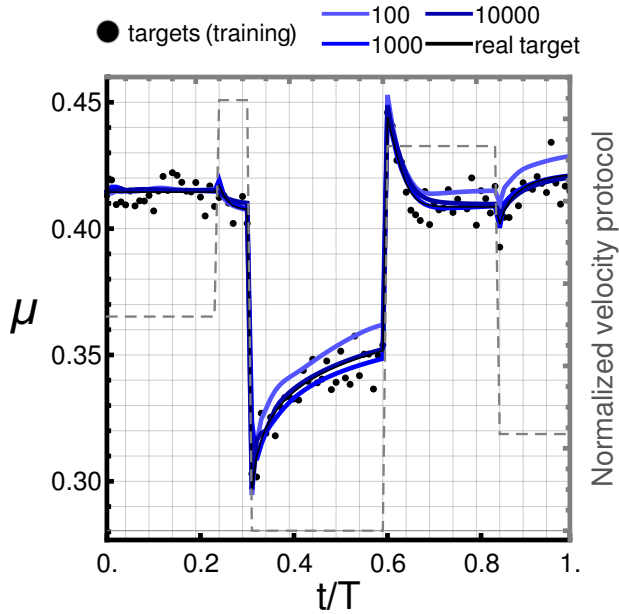


FIG. 4 Test example #2: light right axis for loading velocity, dark right axis for friction coefficient evolution. Emphasis on capacities of neural network based on aging-law datasets (100, 1000 and 10000 sequences). The dashed background line represents the velocity protocol.

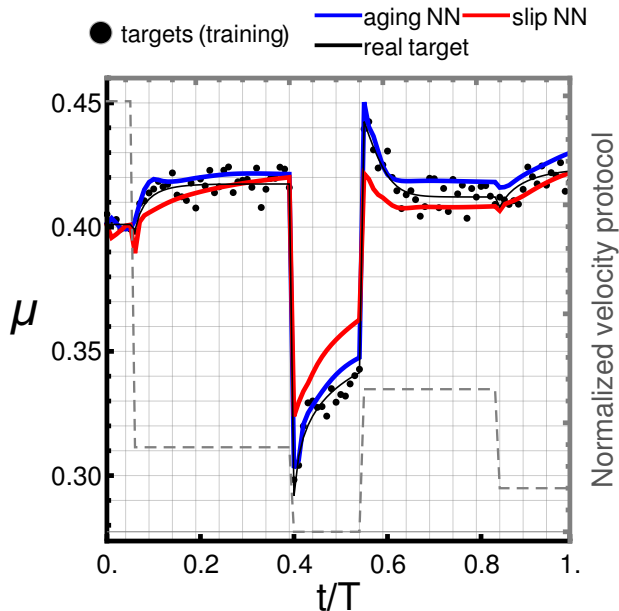


FIG. 5 Test example #3: light right axis for loading velocity, dark right axis for friction coefficient evolution. Emphasis on comparing network trained in slip-law dataset and aging-law dataset for the same amount of training sequences (100). The dashed background line represents the velocity protocol. Protocol with relevant hold.

in terms of network hyperparameters are also warranted, in particular in terms of network depth (e.g., stacking GRUs in different ways³⁹ to make each focus on capturing different phenomena).

Unlike cheap synthetic data, experimental data remains relatively scarce; hence it is worth exploring how

new techniques^{67,68}, aimed at improving data economy in the context of constitutive modeling with neural networks, can help in this case. It is reassuring for the future steps to know that just dozens of experiments (in lieu of hundreds or thousands of them) may be enough to learn interface dynamics. These volumes of information can be generated by isolated laboratories, without requiring large-scale multi-group collaborations. Notwithstanding that, we venture the possibility of coordination between experimentalists to generate richer datasets that can confidently be used to train models for particular interface conditions.

Incorporating spring-block dynamics and stick-slip² into the model will be another step for learning from real laboratory data beyond gouge experiments, thus considering other type of interfaces as e.g. those in PMMA friction.

Moreover, the exploration of advanced machine learning features such as transformers⁶⁹ and Long Short-Term Memory (LSTM) networks⁷⁰ could offer additional improvements. These technologies might provide the key to overcoming some of the technical current limitations (e.g., having to work with fixed-length sequences). The promise of deep learning does not stop there. On one hand, universal models of friction based on minimal state cells⁴⁷ could allow modeling different material interfaces with a single numerical tool; on the other hand, one can foresee that an approach based on neural operators⁷¹ may help also with discretization dependence, having different data sampling frequencies, and with the problem of generalizing friction from lab conditions to crustal ones.

The end goal is to evolve from traditional phenomenological friction models towards more accurate representations that are likewise derived from the data already used for parameter fitting. This evolution does not entail giving up on a deeper understanding of friction dynamics. Rather, it calls for a complementary integration of solid physical principles with the deep-learning paradigm. The rationale for adopting these deep-learning models shall be their demonstrable ability to accurately capture complex interface physics, which, in turn, would justify their use in larger-scale numerical simulations involving those phenomena.

ACKNOWLEDGEMENTS

The author acknowledges financial support from the Swiss National Science Foundation, via Ambizione Grant PZ00P2.216341 “Data-Driven Computational Friction”. Useful conversations (regarding text improvements, rate-and-state friction and/or laboratory experiments) with Dr. Gabriel Meyer, Dr. Simon Guérin-Marthe and Ms. Roxane Ferry are gratefully acknowledged. An EPFL bachelor project conducted by Mr. Antoine Binggeli developed Tensorflow code that inspired the use of GRUs to this particular problem.

Finally, this paper not only verses on but also benefited from artificial intelligence: GPT-4 has provided both help with and input to the text.

DATA AVAILABILITY

The notebooks used to generate both data and results in this paper are available via correspondence with the author (joaquin.garciasuarez@epfl.ch).

REFERENCES

- ^a) Electronic mail: joaquin.garciasuarez@epfl.ch
- ¹E. Rabinowicz, “The Nature of the Static and Kinetic Coefficients of Friction,” *Journal of Applied Physics* **22**, 1373–1379 (1951).
 - ²C. H. Scholz, *The mechanics of earthquakes and faulting* (Cambridge university press, 2019).
 - ³A. Dyson, “Scuffing - a review,” *Tribology International* **8**, 77–87 (1975).
 - ⁴Z. Bažant and B. Oh, “Crack band theory for fracture of concrete,” *Materials and Structures* **16**, 155–177 (1983).
 - ⁵P. Berthoud, T. Baumberger, C. G’Sell, and J.-M. Hiver, “Physical analysis of the state- and rate-dependent friction law: Static friction,” *Phys. Rev. B* **59**, 14313–14327 (1999).
 - ⁶P. K. Mehta and P. J. Monteiro, *Concrete: Microstructure, Properties, and Materials*, 4th ed. (McGraw-Hill Education, New York, NY, 2014).
 - ⁷C. Marone, “Laboratory-derived friction laws and their application to seismic faulting,” *Annual Review of Earth and Planetary Sciences* **26**, 643–696 (1998).
 - ⁸J. Woodhouse, T. Putelat, and A. McKay, “Are there reliable constitutive laws for dynamic friction?” *Philosophical Transactions of the Royal Society A: Mathematical, Physical and Engineering Sciences* **373**, 20140401 (2015).
 - ⁹J. Rice and Y. Ben-Zion, “Slip complexity in earthquake fault models,” *Proceedings of the National Academy of Sciences* **93**, 3811–3818 (1996).
 - ¹⁰J. Dieterich, “Modeling of rock friction: 1. experimental results and constitutive equations,” *Journal of Geophysical Research* **84**, 2161–2168 (1979).
 - ¹¹A. Ruina, “Slip instability and state variable friction laws,” *Journal of Geophysical Research: Solid Earth* **88**, 10359–10370 (1983).
 - ¹²K. L. Johnson, *Contact Mechanics* (Cambridge University Press, Cambridge, UK, 1985).
 - ¹³A. Bizzarri, “On the deterministic description of earthquakes,” *Reviews of Geophysics* **48** (2010).
 - ¹⁴N. M. Beeler, T. E. Tullis, M. L. Blanpied, and J. D. Weeks, “Frictional behavior of large displacement experimental faults,” *Journal of Geophysical Research: Solid Earth* **101**, 8697–8715 (1996), <https://agupubs.onlinelibrary.wiley.com/doi/pdf/10.1029/96JB00411>.
 - ¹⁵C. Marone and B. Kilgore, “Scaling of the critical slip distance for seismic faulting with shear strain in fault zones,” *Nature* **362**, 618–621 (1993).
 - ¹⁶J. H. Dieterich and B. D. Kilgore, “Direct observation of frictional contacts: New insights for state-dependent properties,” *Pure and applied geophysics* **143**, 283–302 (1994).
 - ¹⁷T. Baumberger and C. Caroli, “Solid friction from stick–slip down to pinning and aging,” *Advances in Physics* **55**, 279–348 (2006), <https://doi.org/10.1080/00018730600732186>.
 - ¹⁸P. Bhattacharya, A. M. Rubin, and N. M. Beeler, “Does fault strengthening in laboratory rock friction experiments really depend primarily upon time and not slip?” *Journal of Geophysical Research: Solid Earth* **122**, 6389–6430 (2017).
 - ¹⁹P. Bhattacharya, A. M. Rubin, T. E. Tullis, N. M. Beeler, and K. Okazaki, “The evolution of rock friction is more sensitive to slip than elapsed time, even at near-zero slip rates,” *Proceedings of the National Academy of Sciences* **119**, e2119462119 (2022), <https://www.pnas.org/doi/pdf/10.1073/pnas.2119462119>.
 - ²⁰J. R. Rice and A. L. Ruina, “Constitutive relations for fault slip and earthquake instabilities,” *Pure and Applied Geophysics PA-GEOPH* **121**, 443–475 (1983).
 - ²¹N. Lapusta, J. R. Rice, Y. Ben-Zion, and G. Zheng, “Elastodynamic analysis for slow tectonic loading with spontaneous rupture episodes on faults with rate- and state-dependent friction,” *Journal of Geophysical Research: Solid Earth* **105**, 23765–23789 (2000).
 - ²²H. Noda and N. Lapusta, “Stable creeping fault segments can become destructive as a result of dynamic weakening,” *Nature* **493**, 518–521 (2013).
 - ²³D. M. Veedu and S. Barbot, “The parkfield tremors reveal slow and fast ruptures on the same asperity,” *Nature* **532**, 361–365 (2016).
 - ²⁴S. Xu, E. Fukuyama, F. Yamashita, K. Mizoguchi, S. Takizawa, and H. Kawakata, “Strain rate effect on fault slip and rupture evolution: Insight from meter-scale rock friction experiments,” *Tectonophysics* **733**, 209–231 (2018), physics of Earthquake Rupture Propagation.
 - ²⁵Y. Urata, F. Yamashita, E. Fukuyama, H. Noda, and K. Mizoguchi, “Apparent dependence of rate-and state-dependent friction parameters on loading velocity and cumulative displacement inferred from large-scale biaxial friction experiments,” *Earthquakes and Multi-hazards Around the Pacific Rim, Vol. I*, 23–43 (2018).
 - ²⁶K. Im, D. Saffer, C. Marone, and J.-P. Avouac, “Slip-rate-dependent friction as a universal mechanism for slow slip events,” *Nature Geoscience* **13**, 705–710 (2020).
 - ²⁷A. M. Rubin and J.-P. Ampuero, “Earthquake nucleation on (aging) rate and state faults,” *Journal of Geophysical Research: Solid Earth* **110** (2005).
 - ²⁸Y. Bar-Sinai, E. A. Brener, and E. Bouchbinder, “Stable sliding and velocity-strengthening friction: Nucleation theory versus experiments,” *Geophysical Research Letters* **39** (2012).
 - ²⁹A. Bizzarri, A. Petri, and A. Baldassarri, “Earthquake dynamics constrained from laboratory experiments: new insights from granular materials,” arXiv preprint arXiv:2401.10595 (2024).
 - ³⁰B. Ferdowsi and A. M. Rubin, “A granular physics-based view of fault friction experiments,” *Journal of Geophysical Research: Solid Earth* **125**, e2019JB019016 (2020), e2019JB019016 10.1029/2019JB019016.
 - ³¹B. Ferdowsi and A. M. Rubin, “Slide-hold-slide protocols and frictional healing in discrete element method (dem) simulations of granular fault gouge,” *Journal of Geophysical Research: Solid Earth* **126**, e2021JB022125 (2021), e2021JB022125 2021JB022125.
 - ³²Y. Ben-Zion, “Dynamic ruptures in recent models of earthquake faults,” *Journal of the Mechanics and Physics of Solids* **49**, 2209–2244 (2001).
 - ³³I. Goodfellow, Y. Bengio, and A. Courville, *Deep Learning* (MIT Press, 2016).
 - ³⁴Y. LeCun, Y. Bengio, and G. Hinton, “Deep learning,” *Nature* **521**, 436–444 (2015).
 - ³⁵S. Hochreiter and J. Schmidhuber, “Long short-term memory,” *Neural Computation* **9**, 1735–1780 (1997).
 - ³⁶K. Cho *et al.*, “Learning phrase representations using rnn encoder-decoder for statistical machine translation,” in *Proceedings of the 2014 Conference on Empirical Methods in Natural Language Processing (EMNLP)* (2014).
 - ³⁷Y. Bengio, P. Simard, and P. Frasconi, “Learning long-term dependencies with gradient descent is difficult,” *IEEE Transactions on Neural Networks* **5**, 157–166 (1994).
 - ³⁸M. Raissi, P. Perdikaris, and G. Karniadakis, “Physics-informed neural networks: A deep learning framework for solving forward and inverse problems involving nonlinear partial differential equations,” *Journal of Computational Physics* **378**, 686–707 (2019).
 - ³⁹M. Mozaffar, R. Bostanabad, W. Chen, K. Ehmann, J. Cao, and M. A. Bessa, “Deep learning predicts path-dependent plasticity,” *Proceedings of the National Academy of Sciences* **116**, 26414–26420 (2019).

- ⁴⁰A. Frankel, R. Jones, C. Alleman, and J. Templeton, “Predicting the mechanical response of oligocrystals with deep learning,” *Computational Materials Science* **169**, 109099 (2019).
- ⁴¹Y. Heider, K. Wang, and W. Sun, “So(3)-invariance of informed-graph-based deep neural network for anisotropic elastoplastic materials,” *Computer Methods in Applied Mechanics and Engineering* **363**, 112875 (2020).
- ⁴²M. B. Gorji, M. Mozaffar, J. N. Heidenreich, J. Cao, and D. Mohr, “On the potential of recurrent neural networks for modeling path dependent plasticity,” *Journal of the Mechanics and Physics of Solids* **143**, 103972 (2020).
- ⁴³F. Masi, I. Stefanou, P. Vannucci, and V. Maffi-Berthier, “Thermodynamics-based artificial neural networks for constitutive modeling,” *Journal of the Mechanics and Physics of Solids* **147**, 104277 (2021).
- ⁴⁴H. J. Logarzo, G. Capuano, and J. J. Rimoli, “Smart constitutive laws: Inelastic homogenization through machine learning,” *Computer Methods in Applied Mechanics and Engineering* **373**, 113482 (2021).
- ⁴⁵K. Xu, D. Z. Huang, and E. Darve, “Learning constitutive relations using symmetric positive definite neural networks,” *Journal of Computational Physics* **428**, 110072 (2021).
- ⁴⁶X. He and J.-S. Chen, “Thermodynamically consistent machine-learned internal state variable approach for data-driven modeling of path-dependent materials,” *Computer Methods in Applied Mechanics and Engineering* **402**, 115348 (2022), a Special Issue in Honor of the Lifetime Achievements of J. Tinsley Oden.
- ⁴⁷C. Bonatti and D. Mohr, “One for all: Universal material model based on minimal state-space neural networks,” *Science Advances* **7**, eabf3658 (2021).
- ⁴⁸J. Dornheim, L. Morand, H. J. Nallani, and D. Helm, “Neural networks for constitutive modeling: From universal function approximators to advanced models and the integration of physics,” *Archives of Computational Methods in Engineering* (2023).
- ⁴⁹R. Ishiyama, E. Fukuyama, and B. Enescu, “Estimation of time-variable friction parameters using machine learning,” *Geophysical Journal International* **236**, 395–412 (2023).
- ⁵⁰L. Breiman, “Random forests,” *Machine learning* **45**, 5–32 (2001).
- ⁵¹N. Lapusta and J. R. Rice, “Nucleation and early seismic propagation of small and large events in a crustal earthquake model,” *Journal of Geophysical Research: Solid Earth* **108** (2003).
- ⁵²C. Cattania, S. Hainzl, F. Roth, and L. Wang, “The relationship between slip and aftershocks: A study based on coulomb-rate-and-state models,” *Journal Geophys. Res.* **16**, 5118 (2014).
- ⁵³B. Rouet-Leduc, C. Hulbert, D. C. Bolton, C. X. Ren, J. Riviere, C. Marone, R. A. Guyer, and P. A. Johnson, “Estimating fault friction from seismic signals in the laboratory,” *Geophysical Research Letters* **45**, 1321–1329 (2018).
- ⁵⁴C. Hulbert, B. Rouet-Leduc, P. A. Johnson, C. X. Ren, J. Riviere, D. C. Bolton, and C. Marone, “Similarity of fast and slow earthquakes illuminated by machine learning,” *Nature Geoscience* **12**, 69–74 (2019).
- ⁵⁵K. Wang, C. W. Johnson, K. C. Bennett, and P. A. Johnson, “Predicting future laboratory fault friction through deep learning transformer models,” *Geophysical Research Letters* **49**, e2022GL098233 (2022).
- ⁵⁶S. Karimpouli, D. Caus, H. Grover, P. Martínez-Garzón, M. Bohnhoff, G. C. Beroza, G. Dresen, T. Goebel, T. Weigel, and G. Kwiatek, “Explainable machine learning for labquake prediction using catalog-driven features,” *Earth and Planetary Science Letters* **622**, 118383 (2023).
- ⁵⁷K. Wang and W. Sun, “Meta-modeling game for deriving theory-consistent, microstructure-based traction-separation laws via deep reinforcement learning,” *Computer Methods in Applied Mechanics and Engineering* **346**, 216–241 (2019).
- ⁵⁸M. Cravero Baraja and K. Bhattacharya, “Learning the effective adhesive properties of heterogeneous substrates,” *Extreme Mechanics Letters* **65**, 102110 (2023).
- ⁵⁹P. Thakolkaran, A. Joshi, Y. Zheng, M. Flaschel, L. De Lorenzis, and S. Kumar, “Nn-euclid: Deep-learning hyperelasticity without stress data,” *Journal of the Mechanics and Physics of Solids* **169**, 105076 (2022).
- ⁶⁰M. Flaschel, S. Kumar, and L. De Lorenzis, “Automated discovery of generalized standard material models with euclid,” *Computer Methods in Applied Mechanics and Engineering* **405**, 115867 (2023).
- ⁶¹A. Vakis, V. Yastrebov, J. Scheibert, L. Nicola, D. Dini, C. Minfray, A. Almqvist, M. Paggi, S. Lee, G. Limbert, J. Molinari, G. Ancaux, R. Aghababaei, S. Echeverri Restrepo, A. Papanigelo, A. Cammarata, P. Nicolini, C. Putignano, G. Carbone, S. Stupkiewicz, J. Lengiewicz, G. Costagliola, F. Bosia, R. Guarino, N. Pugno, M. Müser, and M. Ciavarella, “Modeling and simulation in tribology across scales: An overview,” *Tribology International* **125**, 169–199 (2018).
- ⁶²A. Paszke, S. Gross, F. Massa, A. Lerer, J. Bradbury, G. Chanan, T. Killeen, Z. Lin, N. Gimelshein, L. Antiga, A. Desmaison, A. Kopf, E. Yang, Z. DeVito, M. Raison, A. Tejani, S. Chilamkurthy, B. Steiner, L. Fang, J. Bai, and S. Chintala, “Pytorch: An imperative style, high-performance deep learning library,” in *Advances in Neural Information Processing Systems*, Vol. 32, edited by H. Wallach, H. Larochelle, A. Beygelzimer, F. d'Alché-Buc, E. Fox, and R. Garnett (Curran Associates, Inc., 2019).
- ⁶³D. P. Kingma and J. Ba, “Adam: A method for stochastic optimization,” (2017), arXiv:1412.6980 [cs.LG].
- ⁶⁴S. Augustine, *Confessions*, edited by H. Chadwick (Oxford University Press, 1991) book II, Chapter 4.
- ⁶⁵S. Augustine, *The City of God Against the Pagans*, edited by R. W. Dyson (Penguin Books, 2003) book XIX, Chapter 16.
- ⁶⁶A. G. Baydin, B. A. Pearlmutter, A. A. Radul, and J. M. Siskind, “Automatic differentiation in machine learning: a survey,” *Journal of Machine Learning Research* **18**, 1–43 (2018).
- ⁶⁷Z. Yu, S. Ye, Y. Sun, H. Zhao, and X.-Q. Feng, “Deep learning method for predicting the mechanical properties of aluminum alloys with small data sets,” *Materials Today Communications* **28**, 102570 (2021).
- ⁶⁸F. Masi and I. Einav, “Neural integration for constitutive equations using small data,” *Computer Methods in Applied Mechanics and Engineering* **420**, 116698 (2024).
- ⁶⁹A. Vaswani, N. Shazeer, N. Parmar, J. Uszkoreit, L. Jones, A. N. Gomez, L. u. Kaiser, and I. Polosukhin, “Attention is all you need,” in *Advances in Neural Information Processing Systems*, Vol. 30, edited by I. Guyon, U. V. Luxburg, S. Bengio, H. Wallach, R. Fergus, S. Vishwanathan, and R. Garnett (Curran Associates, Inc., 2017).
- ⁷⁰Y. Yu, X. Si, C. Hu, and J. Zhang, “A Review of Recurrent Neural Networks: LSTM Cells and Network Architectures,” *Neural Computation* **31**, 1235–1270 (2019).
- ⁷¹Z. Li, N. Kovachki, K. Azizzadenesheli, B. Liu, K. Bhattacharya, A. Stuart, and A. Anandkumar, “Fourier neural operator for parametric partial differential equations,” (2021).
- ⁷²S. Wolfram, *The mathematica book*, Vol. 4 (Cambridge University Press Cambridge, 2000).
- ⁷³Initial parameters from ME+ICs.
- ⁷⁴Initial parameters from ME+ICs.

Appendix A: Initial tests

The simpler preliminary studies were performed in Mathematica⁷² only for the aging law, eq. (2a). Mathematica’s automatic differentiation capabilities are limited, so alternative implementations of the loss had to be explored.

1. Architecture

The main net is made up by a single `GatedRecurrentLayer`, followed by a folded `LinearLayer`. It is the closest implementation in Mathematica to the architecture used in pyTorch.

a. Training parameters

We employ the ADAM optimization method⁶³ with learning rate of 0.001, batch size of 32, and 50 epochs of training (no early stop, no gradient clipping).

b. Loss function

The first part of the loss is the mean-squared error (MSE):

$$\text{loss}_1 = \frac{\|\delta\boldsymbol{\mu} - \delta\hat{\boldsymbol{\mu}}\|_2^2}{N}, \quad (\text{A1})$$

where $\|\cdot\|_2$ represents the L_2 norm of the vector. In overall graph for training, fig. A.4, this operation is implemented by the neuron labeled MS. This preliminary study revealed a better performance of MAE, eq. (4).

The second part of the loss represents the difference between the initial values of predictions and targets, eq. (5). The implementation of this operation is depicted in fig. A.1: it takes the first sequence value of both targets (`Targets`) and predictions (`Predictions`), subtracts each other and squares the difference.

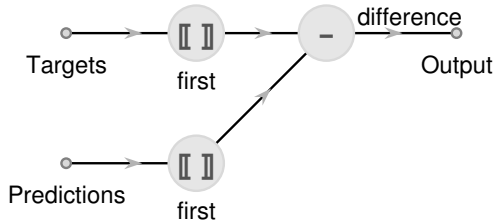


FIG. A.1 Scheme of sub-net that implements comparison of initial condition.

The third term of the loss in this case was meant to enforce the direct effect. Assume that there are N_J jumps in a given protocol, the term that measures the error between the one predicted by the network and the real one is

$$\text{loss}_3 = \sum_{i=1}^{N_J} \{\Delta(\delta\mu)_{J_i} - \Delta(\delta\hat{\mu})_{J_i}\}^2, \quad (\text{A2})$$

the symbol i indexes each jump, while J_i refers to the entry of the vector where the jump begins, hence the meaning of the notation $\Delta(\delta\mu)_{J_i} = \delta\mu_{J_i+1} - \delta\mu_{J_i}$. The network depicted in fig. A.2 implements this procedure: the inputs are the predictions generated by the GRU net, the indices of the entries where velocity jumps begin `PosBeforeJ` and after `PosAfterJ`, and the real magnitude of the friction jump ΔF_{data} , the output is the evaluation of eq. (9), which does not require preprocessing the data and whose implementation is more elegant and way less convoluted.

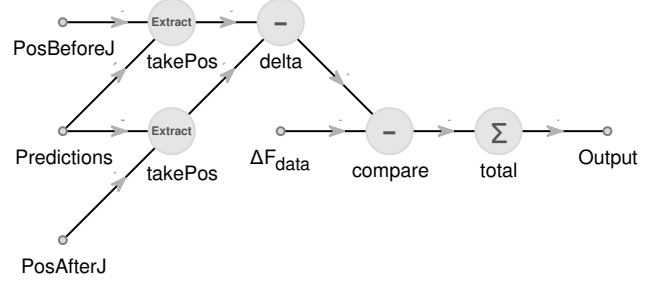


FIG. A.2 Sub-net that implements direct effect.

Finally, interface strengthening during hold periods (a.k.a. healing) is recognized to happen logarithmically with respect to hold time, i.e., counting from the moment that the interface ceases to move. Consider that, given a sequence, the hold period starts at the j -th entry, and it lasts until $(j + N_h)$ -th entry. We can gather these terms in a separate vector $\delta\boldsymbol{\mu}_h = \{\delta\mu_i\}_{i=k}^{i=k+N_h} = \{\delta\mu_n\}_{n=1}^{n=N_h}$, where the sub-index n has been introduced to index the values during hold straightforwardly. Recall that the sampling time step is constant, then we can replace working with time by working with indices. So the healing condition can be expressed as:

$$\frac{\delta\mu_n - \delta\mu_{N_h}}{\log\left(\frac{n}{N_h}\right)} = \text{constant} \quad \forall n = 1, \dots, N_h - 1. \quad (\text{A3})$$

Thus, the loss term is:

$$\text{loss}_4 = \sum_{n=1}^{N_h-2} \left\{ \frac{\delta\mu_{n+1} - \delta\mu_{N_h}}{\log\left(\frac{n+1}{N_h}\right)} - \frac{\delta\mu_n - \delta\mu_{N_h}}{\log\left(\frac{n}{N_h}\right)} \right\}^2. \quad (\text{A4})$$

This loss term is realized schematically as in fig. A.3. The first input is again `Predictions`, coming from the main network, the second one is N_h , which is the position of the entry where the hold ends, it is necessary to extract the predicted value $\delta\mu_{N_h}$. The latter is then replicated to form a vector that is subtracted to all predictions. The final input `LogTerms` weights the healing values as per eq. (A3) and “masks” the not-healing ones since it contains zeros that multiply those entries. Once the vector has been weighted, two copies of it are made, shifted to compare successive entries and then summed and squared, yielding as output eq. (A4).

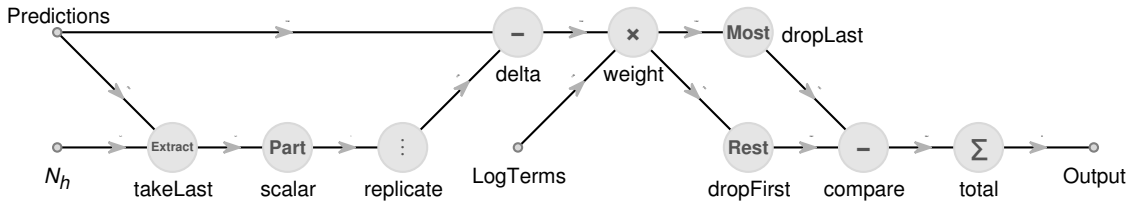


FIG. A.3 Sub-net that implements logarithmic healing during holds.

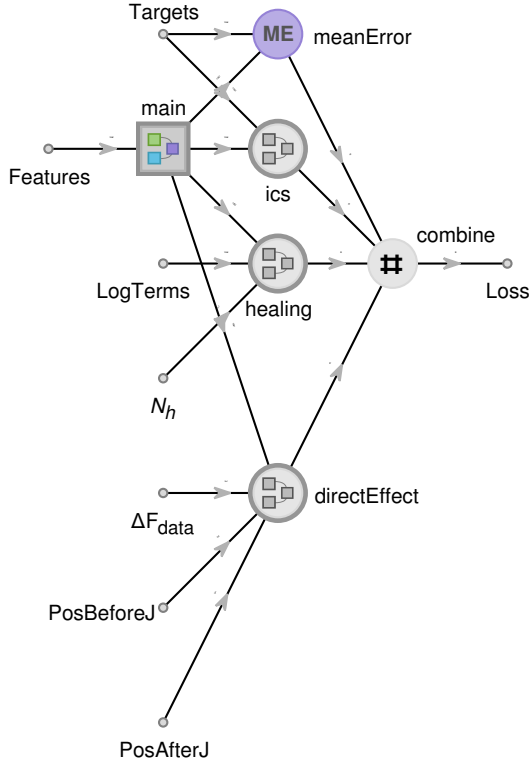


FIG. A.4 Scheme of the global training network

The overall loss term that guides the optimization of weights and biases during the training process is:

$$\text{loss} = \text{loss}_1 + \alpha \text{loss}_2 + \beta \text{loss}_3 + \gamma \text{loss}_4, \quad (\text{A5})$$

$\alpha, \beta, \gamma \in \mathbb{R}$. It was found that $\alpha = 1$, $\beta = 0.1$ and $\gamma = 5 \cdot 10^{-3}$ yields satisfactory results, which at the time were recognized as suboptimal and subsequently improved by the move to pyTorch.

2. Training and validation results

The training was performed using 12000 random sequences corresponding to virtual protocols.

The final losses are consigned in table III.

The complex loss function eq. (A4) was not used at once, but an incremental approach was explored: first, the simplest loss (mean squared error, ME) was used to initialize weights and biases. Second, the network was retrained adding the initial-condition term (ME + ics), which further reduced the loss by 50%. This main part

was again extracted and used into a larger scheme that included the direct effect loss term (ME + ics + de). The overall precision suffered, but, as it will be shown, this deterioration of the objective function minimization does not translate into a substantial deterioration of the overall approximation; rather, it seems that this larger value reflects the struggle to capture the jumps' magnitude. Re-training the network from ME + ics for both direct effect and healing simultaneously (ME + ics + de + heal) was tried, to no avail. The addition of the healing phenomenology to the loss further defects from the optimum, but this could just be a drawback of the RSF model used to generate the synthetic data.

TABLE III Final loss value for different loss functions: ME refers to mean squared error between predictions and targets, ICs refers to enforcing the first value of predictions to be equal to targets', DE does to enforcing friction jumps in target data and predictions to be of the same magnitude, H refers to enforcing logarithmic healing.

| ME | ME+ICs | ME+ICs+DE ⁷³ | ME+ICs+DE+H ⁷⁴ |
|-------|--------|-------------------------|---------------------------|
| 0.064 | 0.033 | 0.255 | 0.271 |

The mean test error (averaged over the 3000 sequences) is consigned in table IV for the four different architectures discussed above. It remains fairly constant, always below 5%, the minimum being attained for the loss combining the averaged square error for the whole vector with the direct enforcement of zero change at $t = 0$. Their accuracy can be directly grasped in figs. 3 and 4, which will be commented in the next section.

Finally, fig. A.5 compares the error distribution across sequences for both the simplest network and the most complex one. In the latter case, the most current error is $\sim 3\%$ (19% of tests), while $\sim 2\%$ (16% of tests) in the former.

TABLE IV Mean test error (%) for different loss functions (see table III for labels' explanation).

| ME | ME+ICs | ME+ICs+DE | ME+ICs+DE+H |
|-----|--------|-----------|-------------|
| 4.2 | 3.4 | 3.7 | 4.1 |

First, the inset in fig. A.6 reveals that the enforcement of the initial condition prevents an initial substantial error, but it does not prevent oscillations even though the velocity remains constant.

Second, the absence of the state variable in the dataset

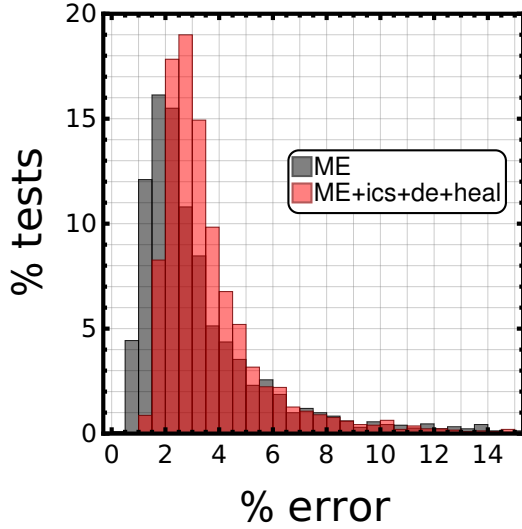


FIG. A.5 Verification error breakdown: percentage of test cases that yield a certain percent error.

brings about limitations in reproducing behavior during holds, despite (or rather, because of) explicitly implementing logarithmic healing in the objective function. This is evinced in fig. A.7 (see inset). Logarithmic healing, eq. (7), entails that the increment of static friction coefficient $\Delta\mu_s$ over a timespan Δt abides by

$$\Delta\mu_s \propto \frac{\Delta t}{t}, \quad (\text{A6})$$

where t is the total time elapsed from the arrest. Conversely, if we integrate eq. (2a) and then plug it back into eq. (1), a term depending on the initial value of the state variable appears:

$$\Delta\mu_s \propto \frac{\Delta t}{\theta(t=0) + t}, \quad (\text{A7})$$

which can interfere with the scaling, unless $\theta(t=0) \ll t$. The latter condition may be met in real experiments, in which the holds tend to last for much longer than the characteristic age of the interface, but it is certainly not the case here as the holds are always “short”, i.e., of duration similar to the magnitude of the state variable.

In any case, this is not an insurmountable drawback, since in laboratory data the behavior during periods of rest would adjust better to the logarithmic scaling.

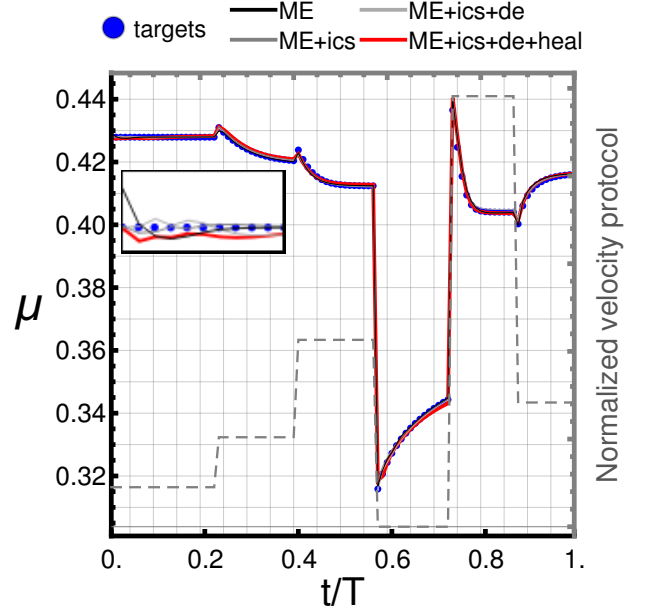


FIG. A.6 Test example #1: light right axis for loading velocity, dark right axis for friction coefficient evolution. Emphasis on initial conditions. The dashed background line represents the velocity protocol. Protocol with hold playing a secondary role.

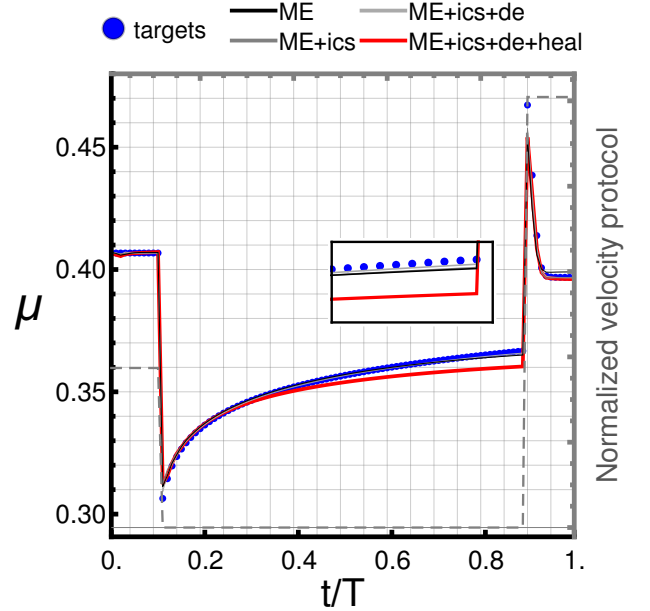


FIG. A.7 Test example #2: light right axis for loading velocity, dark right axis for friction coefficient evolution. Emphasis on shortcomings in healing and direct effect. The dashed background line represents the velocity protocol. Protocol with relevant hold.